DYNAMIC RESPONSE ANALYSIS OF CARRIER-BASED AIRCRAFT DURING LANDING

Duan Pingping(段萍萍)[1,2], *Nie Hong*(聂宏)[1], *Wei Xiaohui*(魏小辉)[1]

(1. State Key Laboratory of Fundamental Mechanical Structure Mechanics and Control, Nanjing University of Aeronautics and Astronautics, Nanjing, 210016, P. R. China;
2. Chengdu Aircraft Design & Research Institute, Aviation Industry Corporation of China, Chengdu, 610091, P. R. China)

Abstract: In view of the complexity of landing on the deck of aircraft carrier, a systematic model, composed of six-degree-of-freedom mathematic model of carrier-based aircraft, four-degree-of-freedom model of landing gears and six-degree-of-freedom mathematic model of carrier, is established in the Matlab-Simulink environment, with damping function of landing gears and dynamic characteristics of tires being considered. The model, where the carrier movement is introduced, is applicable for any abnormal landing condition. Moreover, the equations of motion and relevant parameter are also derived. The dynamic response of aircraft is calculated via the variable step-size Runge-Kuta algorithm. The effect of attitude angles of aircraft and carrier movement during the process of landing is illustrated in details. The analytical results can provide some reference for carrier-based aircraft design and maintenance.

Key words: carrier-based aircraft; landing; carrier movement; dynamic response; landing gear

CLC number: TP391 **Document code**: A **Article ID**: 1005-1120(2013)04-0306-11

INTRODUCTION

By the impacts of carrier air wake and turbulence coming from obstacles upwind of the landing area, the landing motion state and attitudes of aircraft are changeable and complex. In addition, the irregular movements of carrier in waves make the process landing of carrier-based aircrafts more intricate than that of ground-based aircrafts.

Aircraft landing and recovery technology is researched for a half century in foreign countries[1-4]. While study on carrier-based aircraft landing dynamic performance began in 1990s in China and achieved some progress[5-9]. However, in most of them it is assumed that the plane lands symmetrically and the interaction between landing gears and the fuselage is ignored. In Ref. [6], the drop model of single landing gear was built and the effect of the carrier movement on drop impact forces was analyzed. In Ref. [7], the landing gears were simplified as one-degree systems and the impact loads of landing gears were discussed while the carrier moving in regular waves. The analytical results showed the moremement of carrier had influence on the landing loads. In above models, the comprehensive actions between landing gears and fuselage and the aircraft attitude response are ignored.

In this article the systematic dynamics model including aircraft, landing gears and carrier is established. In this model the landing gears have four-degree-of-freedom (DOF), three translational degrees and one rotational degree round the wheel center. The aircraft and the carrier are six-DOF systems. The dynamic response of the aircraft and landing gears is obtained by numerical method and the effects of plane′s initial situation and the movements of carrier are detailed demonstrated. Also, the aerodynamic forces and the

Foundation items: Supported by the National Natural Science Foundation of China (51075203, 51105197); the Research Funding of Nanjing University of Aeronautics and Astronautics (NS2010023).

Received date: 2011-08-04; **revision received date**: 2012-02-20

Corresponding author: Nie Hong, Professor, E-mail: hnie@nuaa.edu.cn.

carrier sailing speed are taken into account. The analytical results are helpful to the study on design criteria and maintenance regulations of carrier-based aircraft.

1 ESTABLISHMENT OF LANDING DYNAMICS MODEL

1.1 Coordinate systems and fundamental assumptions

Several basic coordinate systems are created to facilitate the description of a variety of related parameters, as shown in Fig. 1. $O_g x_g y_g z_g$ is the ground coordinate system fixed to the ground. The origin is a point located on the ground, axis x_g is in the level and parallel to the runway central line while the carrier is still, axis y_g is in the plumb upward direction, and axis z_g is determined by the right hand rule. $O_f x_f y_f z_f$ is the aircraft coordinate system. The origin is placed at the plane mass center, axis x_f is parallel to the center symmetry surface of the aircraft and in the forward direction, axis y_f is in the center symmetry surface and perpendicular to axis x_f, and axis z_f is perpendicular to the center symmetry surface pointing to the right wing. $O_c x_c y_c z_c$ is the carrier coordinate system. The origin is located at the carrier mass center, axis x_c is parallel to the longitudinal central line of the carrier pointing to the prow, axis y_c is perpendicular to the deck plane pointing to the top, axis z_c is perpendicular to the longitudinal central plane pointing to the starboard. $O_d x_d y_d z_d$ is the deck coordinate system. The origin is placed at the designed touchdown point(DTP) in the deck plane, axis x_d is parallel to the runway centerline and in the forward direction, axis y_d is perpendicular to the deck plane pointing to the top, and axis z_d follows the right-hand rule with axes x_d and y_d. $O_{f'} x_{f'} y_{f'} z_{f'}$ is the aircraft-deck coordinate system. The origin is O_d, axis $x_{f'}$ is the projection of axis x_f in the deck plane, axis $y_{f'}$ is perpendicular to the deck plane pointing to the top, and axis $z_{f'}$ follows the right-hand rule. $O_s x_s y_s z_s$ is the strut coordinate system. The origin is placed at the landing gear installation point on the fuselage, axis z_s is along the strut and in the downward direction, axis y_s is parallel to the $y_f z_f$ plane, perpendicular to axis z_s and in the outward direction, and axis x_s is determined by the right hand rule. $O_w x_w y_w z_w$ is the wheel coordinate system. The origin is located at the wheel axle center, axis x_w is parallel to the axis $x_{f'}$ and in the same direction, axis y_w is in the wheel central plane and perpendicular to axis x_w, and axis z_w is determined by right hand rule. ψ is the deck angle, and φ_s and θ_s are the installation angles of the landing gear.

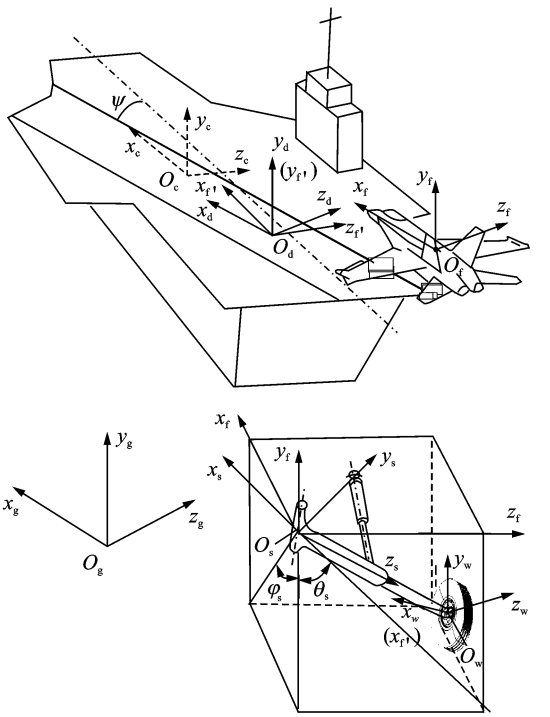

Fig. 1 Sketch of coordinate systems

For simplifying the system and making the system more realizable, the following assumptions are made:

(1) The aircraft body is divided into elastically-supported part and non-elastically-supported part. The former includes the fuselage, the wings and outer cylinders of dampers etc. The latter contains the pistons of dampers, brake devices, wheels and launch bar etc.

(2) The elastically-supported part's motion is six-DOF, non-elastically-supported part's motion is four-DOF, three translational degrees and one rotational degree round the wheel center, and the

mass center is at the wheel axle.

(3) The expansion of absorbers and lateral deformation of pistons are considered, and other deformations of absorber structure are ignored.

(4) The moment that the deck acts on the aircraft body contains the moment from landing gears to the fuselage and the additional moment caused by the translation of tire forces from touchdown points to the wheel axle centers.

1.2 Differential equations of system motion

The force condition of aircraft during landing is shown in Fig. 2. Based on the analysis of the aircraft's working conditions, the equations of motion are built in certain coordinate system.

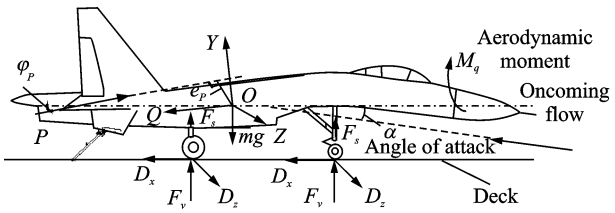

Fig. 2 Sketch of force analysis during landing

(1) The equation of translational motion of the fuselage is built in the aircraft coordinate system[10-11], shown as

$$m\left(\frac{\mathrm{d}}{\mathrm{d}t}\begin{bmatrix}v_{x_\mathrm{f}}\\v_{y_\mathrm{f}}\\v_{z_\mathrm{f}}\end{bmatrix}+\begin{bmatrix}\omega_x\\\omega_y\\\omega_z\end{bmatrix}^{ss}\begin{bmatrix}v_{x_\mathrm{f}}\\v_{y_\mathrm{f}}\\v_{z_\mathrm{f}}\end{bmatrix}\right)=\begin{bmatrix}P\cos\varphi_P\\P\sin\varphi_P\\0\end{bmatrix}+\boldsymbol{T}_\mathrm{a}^\mathrm{f}\begin{bmatrix}-Q\\Y\\Z\end{bmatrix}+\boldsymbol{T}_\mathrm{g}^\mathrm{f}\begin{bmatrix}0\\-mg\\0\end{bmatrix}+\sum_{i=N,L,R}\boldsymbol{T}_{si}^\mathrm{f}\begin{bmatrix}N_{x_{si}}\\N_{y_{si}}\\-F_{si}\end{bmatrix}\tag{1}$$

(2) The equation of rotational motion of the fuselage is built in the aircraft coordinate system, shown as

$$\boldsymbol{I}\frac{\mathrm{d}}{\mathrm{d}t}\begin{bmatrix}\omega_x\\\omega_y\\\omega_z\end{bmatrix}+\begin{bmatrix}\omega_x\\\omega_y\\\omega_z\end{bmatrix}^{ss}\boldsymbol{I}\begin{bmatrix}\omega_x\\\omega_y\\\omega_z\end{bmatrix}=\sum_{i=N,L,R}\begin{bmatrix}R_{x_i}\\R_{y_i}\\R_{z_i}\end{bmatrix}^{ss}\begin{bmatrix}N_{x_{si}}\\N_{y_{si}}\\-F_{si}\end{bmatrix}+\begin{bmatrix}0\\0\\-Pe_P\end{bmatrix}+\frac{1}{2}\rho u^2 S_\mathrm{ref}l_\mathrm{w}\begin{bmatrix}C_{\mathrm{m}_x}\\C_{\mathrm{m}_y}\\C_{\mathrm{m}_z}\end{bmatrix}-\sum_{i=N,L,R}\boldsymbol{T}_\mathrm{w}^\mathrm{f}\begin{bmatrix}0\\\delta_{yi}\\0\end{bmatrix}\left(\boldsymbol{T}_{\mathrm{f}'}^\mathrm{f}\begin{bmatrix}-D_{x_{\mathrm{f}'i}}\\F_{v_{\mathrm{f}'i}}\\-D_{z_{\mathrm{f}'i}}\end{bmatrix}\right)\tag{2}$$

(3) The equation of translational motion of the non-elastically-supported part is built in the aircraft coordinate system, shown as

$$m_1\left(\frac{\mathrm{d}}{\mathrm{d}t}\begin{bmatrix}v_{x_1}\\v_{y_1}\\v_{z_1}\end{bmatrix}+\begin{bmatrix}\omega_x\\\omega_y\\\omega_z\end{bmatrix}^{ss}\begin{bmatrix}v_{x_1}\\v_{y_1}\\v_{z_1}\end{bmatrix}\right)=\boldsymbol{T}_\mathrm{g}^\mathrm{f}\begin{bmatrix}0\\-m_1g\\0\end{bmatrix}+\boldsymbol{T}_\mathrm{s}^\mathrm{f}\begin{bmatrix}N_{x_\mathrm{s}}\\N_{y_\mathrm{s}}\\-F_\mathrm{s}\end{bmatrix}+\boldsymbol{T}_{\mathrm{f}'}^\mathrm{f}\begin{bmatrix}-D_{x_{\mathrm{f}'}}\\F_{v_{\mathrm{f}'}}\\-D_{z_{\mathrm{f}'}}\end{bmatrix}\tag{3}$$

(4) The rotational equation of wheel is built as follows

$$I_\mathrm{w}\frac{\mathrm{d}\omega_\mathrm{w}}{\mathrm{d}t}=(R_0-\delta)D_{x_{\mathrm{f}'}}\tag{4}$$

where $[\omega_x\quad\omega_y\quad\omega_z]^\mathrm{T}$ is the angular velocity of the aircraft coordinate frame; $[P\cos\varphi_P\quad P\sin\varphi_P\quad 0]^\mathrm{T}$ is the engine thrust, φ_P is the angle between the direction of thrust and axis x_f; $[-Q\quad Y\quad Z]^\mathrm{T}$ is the aerodynamic force; $[N_{x_{si}}\quad N_{y_{si}}\quad -F_{si}]^\mathrm{T}$ is the force acted on the fuselage caused by landing gear; $[R_{x_i}\quad R_{y_i}\quad R_{z_i}]^\mathrm{T}$ is the distance from aircraft mass center to wheel axle center; $[C_{\mathrm{m}_x}\quad C_{\mathrm{m}_y}\quad C_{\mathrm{m}_z}]^\mathrm{T}$ is the aerodynamic moment coefficient; $[0\quad\delta_{y_i}\quad 0]^\mathrm{T}$ the distance from the touchdown point on the tire to the wheel axle center; $[-D_{x_{\mathrm{f}'i}}\quad F_{v_{\mathrm{f}'i}}\quad -D_{z_{\mathrm{f}'i}}]^\mathrm{T}$ is the tire force caused by the deck; e_P is the vertical distance from aircraft mass center to the thrust line; u is the airspeed; S_ref is the reference wing area; l_w is the wing span; $\boldsymbol{T}_\mathrm{w}^\mathrm{f}$, $\boldsymbol{T}_{\mathrm{f}'}^\mathrm{f}$, $\boldsymbol{T}_\mathrm{g}^\mathrm{f}$, $\boldsymbol{T}_\mathrm{s}^\mathrm{f}$ are the transformation matrices from the wheel coordinate system, the aircraft-deck coordinate system, the ground coordinate system, and the strut coordinate system to the aircraft coordinate system, respectively.

1.3 Solution of model

The set of system differential equations built above cannot be solved without supplementary equations which includes calculations of landing gear forces, tire forces and aircraft attitude angles.

(1) Calculation model for forces of landing gear

The landing gear forces contain the axial and lateral loads. As show in Eq. (5), the axial force includes the air spring force F_a, the oleo-damping force F_h, the internal frictional force F_f and the structural constraint force F_l.

$$F_s = F_a + F_h + F_l + F_f \tag{5}$$

Ignoring the compressibility of fluid, the air spring force is given by[12]

$$F_a = A_a\left[P_0\left(\frac{V_0}{V_0 - A_a s}\right)^n - P_{atm}\right] \tag{6}$$

Taking the damper with variable main orifice and lateral oil holes as an example, the oleo-damping force is given by

$$F_h = \begin{cases} \dfrac{\rho_{oil} A_h^3 \dot{s}^2}{2C_d^2 A_d^2} + \dfrac{\rho_{oil} A_{hs}^2 \dot{s}^2}{2C_{ds}^2 A_n^2} & \dot{s} \geqslant 0 \\ -\dfrac{\rho_{oil} A_h^3 \dot{s}^2}{2C_d^2 A_d^2} - \dfrac{\rho_{oil} A_{hs}^2 \dot{s}^2}{2C_{ds}^2 A_n^2} & \dot{s} < 0 \end{cases} \tag{7}$$

The structural constraint force is described as follow

$$F_l = \begin{cases} k_1 s & s < 0 \\ 0 & 0 \leqslant s \leqslant s_{max} \\ k_1(s - s_{max}) & s > s_{max} \end{cases} \tag{8}$$

The internal frictional force consists of two parts

$$F_{f1} = \mu_b(N_u + N_l)\frac{\dot{s}}{|\dot{s}|} \tag{9}$$

$$F_{f2} = \mu_b F_0 \frac{\dot{s}}{|\dot{s}|} \tag{10}$$

where F_{f1} is the coulomb friction induced by strut bending; F_{f2} is the sleeve friction induced by internal pressure of chamber.

The lateral strut forces are given by[13]

$$N_{x_s} = k_x f_x + c_x \dot{f}_x \tag{11}$$

$$N_{y_s} = k_y f_y + c_y \dot{f}_y \tag{12}$$

where A_a, A_h, A_d, A_{hs}, A_n are the external sectional areas of the piston rod, the internal net area of piston rod, the net area of main oil orifice, the pushed-oil net area of return-oil chamber, and the orifice area of return-oil chamber respectively; A_d and A_h are the functions of the amount of compression s; P_0, P_{atm} are the initial pressures of low pressure and the atmospheric pressure; V_0, N_u, N_l are the initial volumes of low pressure, the tensions at the upper and lower supporting points; n, ρ_{oil}, C_d, C_{ds}, μ_b are the polytrophic exponents of air compress process, the density of oil, the coefficient of oil contraction in main oil chamber, the coefficient of oil contraction in return-oil chamber and the friction coefficient respectively; and k_x, k_y, c_x, c_y are the lateral stiffness coefficients and damping coefficients.

(2) Calculation model for tire force

The supporting force from the deck is perpendicular to the deck plane

$$F_v = (1 + C_T\dot{\delta})f(\delta) \tag{13}$$

The wheel friction forward is

$$D_x = \mu_x F_v \tag{14}$$

The wheel friction sideward is[14]

$$D_z = \begin{cases} \left(\varphi - \dfrac{4}{27}\varphi^3\right)\mu_z F_v & \varphi < 1.5 \\ \mu_z F_v & \varphi \geqslant 1.5 \end{cases} \tag{15}$$

where C_T, δ, $f(\delta)$ are the wheel vertical damping deformation coefficient, the tire deflection and the tire static-pressure performance respectively; μ_x is the adhesion coefficient in the course direction, depending largely on the tire slipping rate; μ_z is the adhesion coefficient laterally; and φ is a factor highly related to yawing angle, tire tilt angle and F_v.

(3) Calculation model attitude for angles of aircraft

The attitude angles can be achieved from the rotation rate obtained from Eq. (2) using Eq. (16) and by integration, shown as

$$\begin{cases} \dfrac{d\gamma}{dt} = (\omega_z\cos\theta + \omega_y\sin\theta)/\cos\varphi \\ \dfrac{d\varphi}{dt} = \omega_y\cos\theta - \omega_z\sin\theta \\ \dfrac{d\theta}{dt} = \omega_x + \tan\varphi(\omega_z\cos\theta + \omega_y\sin\theta) \end{cases} \tag{16}$$

(4) Calculation of other parameters

The deformation of damper is

$$\begin{bmatrix} f_x \\ f_y \\ -s \end{bmatrix} = \boldsymbol{T}_s^{fT}\left(\boldsymbol{T}_g^f\begin{bmatrix} R_x \\ R_y \\ R_z \end{bmatrix} - \begin{bmatrix} xr_{O_f} \\ yr_{O_f} \\ zr_{O_f} \end{bmatrix}\right) - \begin{bmatrix} 0 \\ 0 \\ l_{s0} \end{bmatrix} \tag{17}$$

The deformation rate is

$$\begin{bmatrix} \dot{f}_{fx} \\ \dot{f}_{fy} \\ -\dot{s} \end{bmatrix} = \boldsymbol{T}_s^{fT}\left(\dot{\boldsymbol{T}}_g^f\begin{bmatrix} R_x \\ R_y \\ R_z \end{bmatrix} + \boldsymbol{T}_g^f\left(\begin{bmatrix} v_{lx} \\ v_{ly} \\ v_{lz} \end{bmatrix} - \begin{bmatrix} v_{x_f} \\ v_{y_f} \\ v_{z_f} \end{bmatrix}\right)\right) \tag{18}$$

where

$$\dot{\boldsymbol{T}}_{\mathrm{g}}^{\mathrm{f}}=\boldsymbol{T}_{\mathrm{g}}^{\mathrm{f}}[\boldsymbol{\omega}_{\mathrm{g}}]^{ss}-[\boldsymbol{\omega}_{\mathrm{f}}]^{ss}\boldsymbol{T}_{\mathrm{g}}^{\mathrm{f}} \tag{19}$$

In the carrier coordinate system, the position vector of the wheel axle center versus the carrier mass center is

$$\begin{bmatrix}R_{x\mathrm{lc}}\\R_{y\mathrm{lc}}\\R_{z\mathrm{lc}}\end{bmatrix}=\boldsymbol{T}_{\mathrm{f}}^{\mathrm{c}}\left(\begin{bmatrix}x_{\mathrm{l}}\\y_{\mathrm{l}}\\z_{\mathrm{l}}\end{bmatrix}-\begin{bmatrix}x_{\mathrm{c}}\\y_{\mathrm{c}}\\z_{\mathrm{c}}\end{bmatrix}\right) \tag{20}$$

The distance from the wheel touchdown point to the wheel axle center is

$$\delta_y=\frac{R_{y\mathrm{lc}}-H}{\cos\Theta} \tag{21}$$

The tire deflection is

$$\delta=\begin{cases}R_0-\delta_y & R_0>\delta_y\\ 0 & R_0\leqslant\delta_y\end{cases} \tag{22}$$

where $\begin{bmatrix}xr_{O_{\mathrm{f}}} & yr_{O_{\mathrm{f}}} & zr_{O_{\mathrm{f}}}\end{bmatrix}^{\mathrm{T}}$, $[R_x \quad R_y \quad R_z]^{\mathrm{T}}$ are the position vectors of the landing gear installation point and the wheel center versus the aircraft mass center; H, R_0, Θ are the height of deck plane above the carrier mass center, the initial radius of wheel and the angle between $O_{y_{\mathrm{f}}}$ axis and $O_{y_{\mathrm{w}}}$ axis (viz. tire tilt angle).

2 EFFECT OF ATTITUDE ANGLES ON DYNAMIC RESPONSE OF AIRCRAFT

After entering the threshold of the glide path, owing to the complex maritime phenomena and wake air zone, the landing attitude is various. The yawing angle, whereas, leads to off-center arresting critically affecting the arresting performance and has little influence on the aircraft vertical dynamic response, therefore the yawing angle is not taken into account.

2.1 Effect of pitching angle

Effects of landing pitching angle on the dynamic response are shown in Fig. 3. In rare cases, due to the ground effect and turbulence off the "island" of ship, the aircraft heads down and lands with a negative pitching angle meaning that the nose landing gear touches down before the main (e.g. $\theta=-6°$ in Fig. 3). In that case, the nose landing gear load surges to 310 kN and the main landing gear load does not decline meanwhile. It is dangerous condition for the nose landing gear. When $\theta=-2°$, three-point landing is achieved nicely, the impact load of main landing gear reaches the minimum and the nose is relatively large as loading at the same time with main gears. In

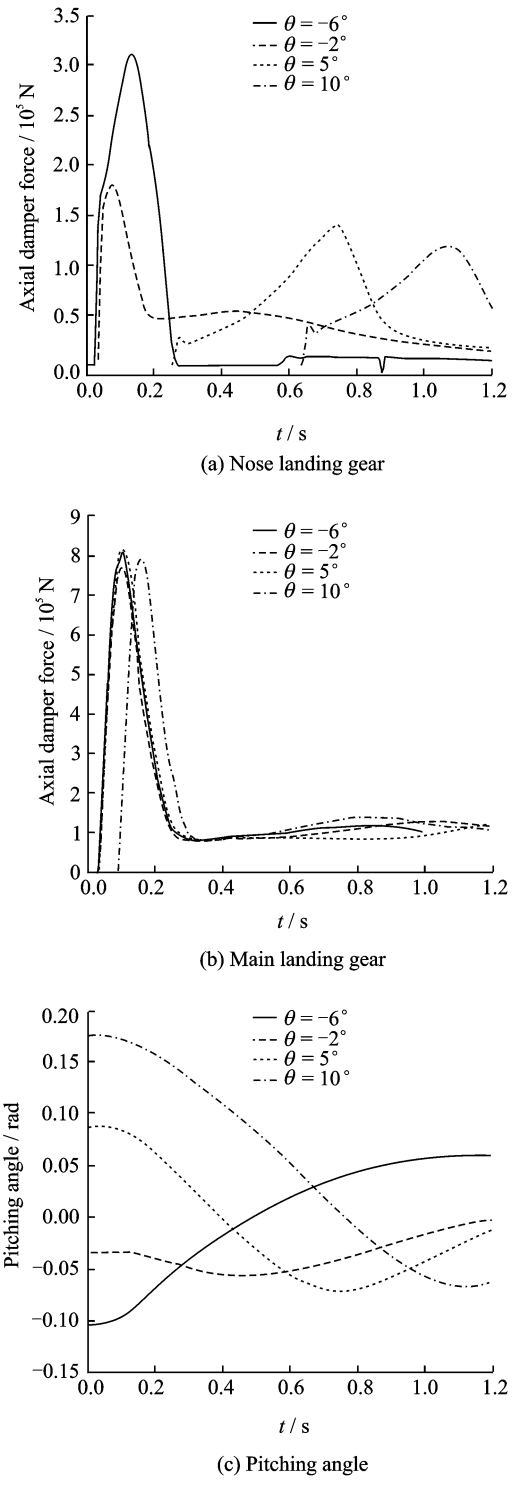

Fig. 3 Dynamic response of aircraft under different landing pitching angles

addition, as the pitching angle increases, the main gear load grows up slightly. Essentially speaking, the pitching angle determines the lag between the touchdown time of nose and main landing gears. The greater the time lag is, the larger the main landing gear load is and the smaller the nose landing gear load is. There are two apparent peaks in the nose landing gear load curve: The touchdown of nose landing gear leads to a positive pitch moment and the nose wheel ascends; the aircraft heads down at the negative pitch moment caused by the main landing gear force, and the nose wheel retouches down afterwards bringing about the second peak. The pitching angle is larger and the effect is more obvious which transfers the maximum value of impact load from first peak to second. The bolting maneuver always occurs for about 1 s after the main landing gear touching down[15]. It is illustrated that as the landing pitching angle increases, the pitching angle is larger at the bolting point of time. This is beneficial to the escape.

2.2 Effect of rolling angle

Effects of rolling angle on dynamic response of aircraft are shown in Fig. 4. As shown in Fig. 4, with the growth of rolling angle, the right landing gear shock load rises. When $\gamma=30°$, the right wheel nearly takes off ground under the negative rolling torque induced by the force-on-right-wheel. The variation of right landing gear impulse load is inconsistent with the change of rolling angle: When the rolling angle increases from 0° to 10°, the landing pattern changes from symmetry to asymmetry, and the impulse load goes up; when the rolling angle increases from 10° to 20°, i. e. delaying the left wheel′s touchdown, the impulse load falls; when $\gamma=30°$, the nose wheel touches down before left wheel, and the left impact load ascends a little whereas the nose impact load jumps dramatically, which should be avoided. Along with the increase of landing rolling angle, the load of aircraft is more asymmetrical and the rolling movement of aircraft is fiercer which is bad for the cable-hook clench and arresting performance.

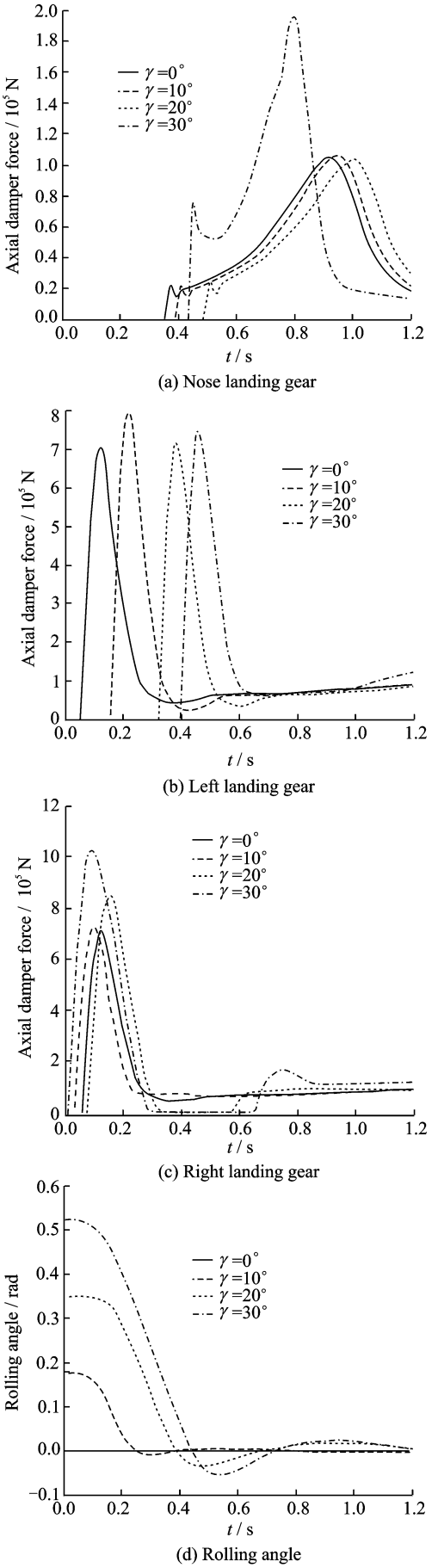

Fig. 4 Dynamic response of aircraft under different landing rolling angles

3 EFFECT OF CARRIER MOVEMENT ON DYNAMIC RESPONSE OF AIRCRAFT

When sailing on the ocean, the carrier movement is six-DOF and irregular under waves and gusts: Swaying, surging, heaving, pitching, rolling and yawing [16]. Three of them have relatively greater influence on the landing of aircrafts[17].

The three movements can be simplified and described using sine function, shown as

$$\begin{cases} \gamma_C = A_\gamma \sin(\omega_\gamma t + \varphi_{\gamma 0}) \\ \theta_C = A_\theta \sin(\omega_\theta t + \varphi_{\theta 0}) \\ h_C = A_h \sin(\omega_h t + \varphi_{h0}) \end{cases} \tag{23}$$

where γ_C, θ_C, h_C are the rolling angle, the pitching angle and the heaving displacement; and A, ω, φ_0 are the corresponding amplitude, frequency and initial phase.

In Ref. [17], when the carrier sailing at a typical speed of 30 kn. The amplitudes of rolling, pitching and heaving are about 6°, 1.05° and 1.5 m respectively. The picked period values are 4, 10, 10 s in this article. The carrier physical and geometric characteristics are taken from Ref. [18].

3.1 Effect of carrier rolling movement

(1)Effect of initial phase of rolling movement

The initial phase of rolling determines the relative velocities between the main wheels and the deck: As the landing zone is on the left of ship longitudinal middle line, when $\varphi_0 = 0$, the relative velocities are greatest; when $\varphi_0 = \pi$, the relative velocities are smallest. When $\varphi_0 = 0$, the landing zone deck goes upward and the velocity of left landing gear touch site is greater than that of the right. When $\varphi_0 = \pi$, the landing zone deck goes downward and velocity of left landing gear touch site remains greater than that of the right. Therefore, the change of left gear impact load is larger than that of the right (Table 1) and the loads of both do not vary too much. As for the nose wheel, the maximum load does not appear at the same initial phase with the main gears. Adjusting the initial phase to make the phase be 0 or π at the time of the second peak of nose load, the extreme values of impact force are obtained. It can be seen that the effect of rolling phase on the nose landing gear impact force is considerable. What's more, when the initial phase is not 0 or π, the aircraft lands asymmetrically which leads the rolling movement of aircraft. It is adverse to the buffering performance of landing gear. Effects of carrieer rolling movement on rolling angle are shown in Fig. 5.

Table 1 Impact loads of landing gears under different phases of carrier movements

Situation		NLG(100 kN)		LLG(100 kN)		RLG(100 kN)	
Ship still		1.50	Growth/%	7.58	Growth/%	7.58	Growth/%
Rolling	0	2.11	+40.7	8.34	+10.03	7.24	−4.49
	π	1.18	−21.3	7.10	−6.33	8.17	+7.78
Pitching	0	1.26	−16.0	4.45	−41.29	4.48	−40.90
	π	2.68	+78.71	1.24	+48.28	11.21	+47.89
Heaving	0	1.89	+26.0	9.92	+30.87	9.92	+30.87
	π	1.22	−18.7	5.57	−26.52	5.57	−26.52

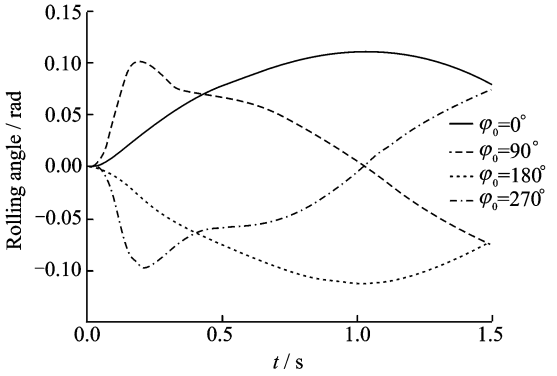

Fig. 5 Rolling angle of aircraft under different initial phases of carrier rolling movement

(2)Effect of period of rolling movement

Fig. 6 represents the loads of landing gears under different periods $T(\varphi_0 = 0)$. Impact loads of main landing gears do not vary in the same trend: As the rolling movement gets more slowly (the period getting greater), the combination velocity between the left landing gear and the deck and the shock load decline; on the contrary, the change of right gear load is getting greater with a relatively smaller extent. With the rise of period, delaying the touchdown of nose landing gear, the

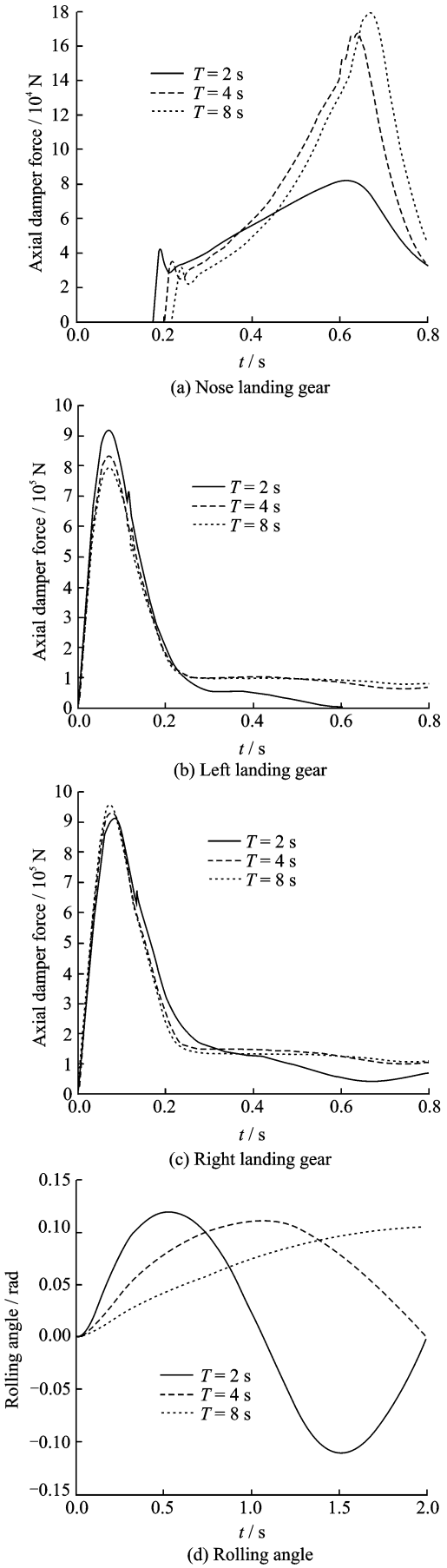

Fig. 6 Dynamic response of aircraft under different carrier rolling periods

rolling phase changes at the time of second leap and the combination velocity between the nose landing gear and the deck gets greater. Also, the more quickly the carrier rolls, the fiercer the aircraft rolls.

3.2 Effect of carrier pitching movement

(1) Effect of initial phase of pitching movement

Because the rolling angle is small and the distances from touchdown sites of main landing gears to the carrier pitching center differ little, the main landing gears almost touchdown simultaneously and the loads change consistently. In Table 1, we can see that unlike rolling, the pitching movement has a great influence on impact loads of both nose and main landing gears. The landing area is at the rearward of the carrier. When $\varphi_0 = 0$, the landing area deck goes downward, the combination velocities of landing gears reduce and vice versa. Obviously, when the carrier pitching angle is positive during landing (the phase is in the range of 0—π), the establishment of attack angle for bolting will get easier. Effects of carrier pitching initial phase on pitching angle are shown in Fig. 7.

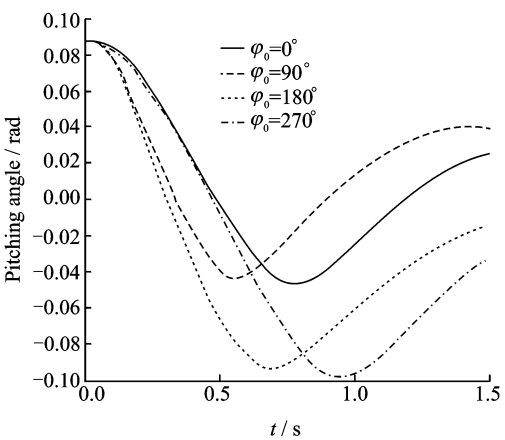

Fig. 7 Pitching angle of aircraft under different carrier pitching initial phases

(2) Effect of period of pitching movement

Effects of period of pitching movement on dynamic response are shown in Fig. 8. When $\varphi_0 = 0$, as the pitching movement becomes slower (the period getting larger), the velocity downward of the landing zone deck reduces, namely the rela-

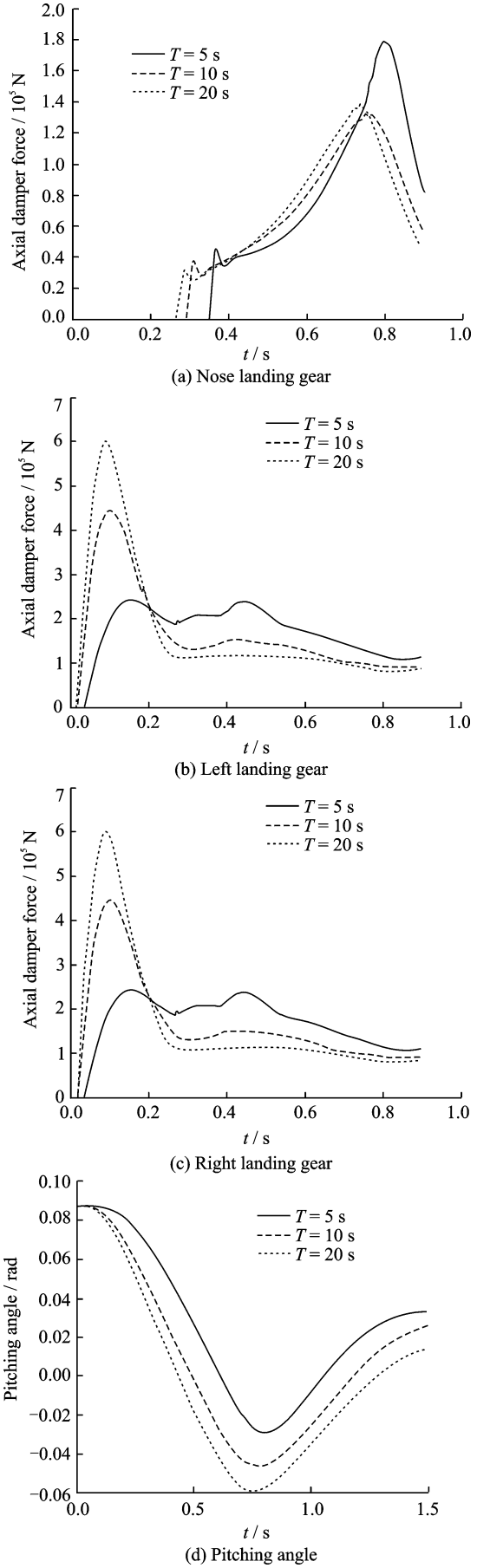

Fig. 8 Dynamic response of aircraft under different periods of carrier pitching movement

tive velocity between the wheels and deck increasing, the impact load goes up. In term of nose landing gear, the speed downward of deck at the moment of second peak declines with a larger period: The load while $T=10$ s is greater than that while $T=20$ s. For the relatively smaller load of main landing gears, when $T=5$ s, the vertical acceleration upward of aircraft decreases, causing the speed of nose wheel at the peak moment larger, and the relative velocity between the wheel and deck is greater than that when $T=20$ s instead. When the pitching movement accelerates, the pitching angle of aircraft is greater at the bolting time which alleviates the pressure of the longitudinal control of aircraft. However this effect is not evident.

3.3 Effect of carrier heaving movement

(1) Effect of initial phase of heaving movement

The heaving movement is vertical and does not lead the asymmetric load between main gears. When $\varphi_0=0$, the carrier goes upward as a whole and the impact speed of aircraft increases. In contrast with rolling and pitching, heaving movement has a smaller effect on the nose landing gear and the effect on the main landing gears is between them.

(2) Effect of period of carrier heaving movement

Similarly, the growth of period makes the vertical speed of carrier fall and the combination velocity of aircraft declines thereby, both the nose and the main landing gear load decrease. In this sense, the heaving period is analogous to the subsidence velocity. The effect of heaving on pitching angle of aircraft is just like pitching but with a smaller degree, shown as Fig. 9.

4 CONCLUSIONS

Considering the aerodynamic force and the carrier sailing speed, the complete landing impact model is built in this article. The calculation and analysis are performed to study the response of aircraft under different situations. The conclusions are drawn below:

(1) Different aircraft attitudes correspond to

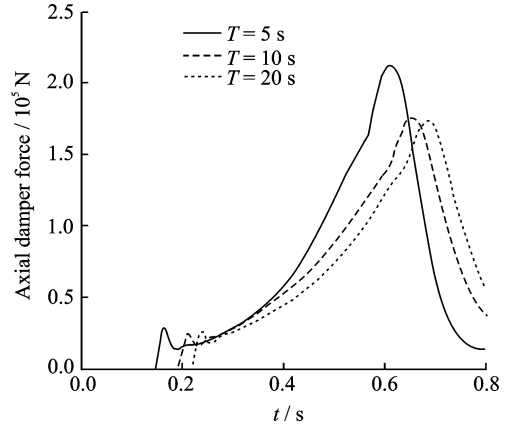

(a) Nose landing gerar

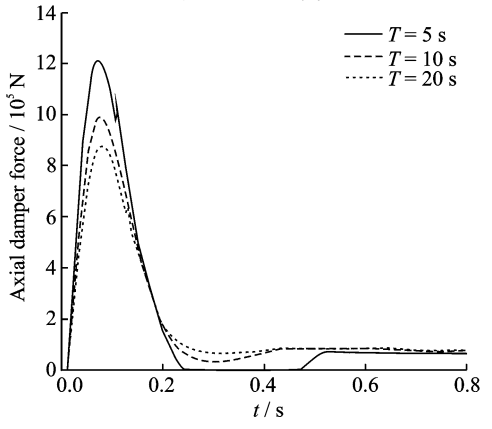

(b) Left landing gear

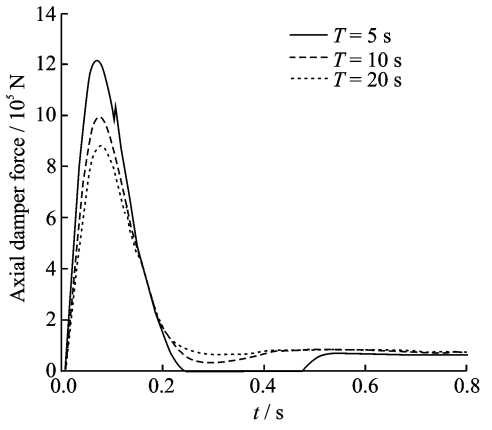

(c) Right landing gear

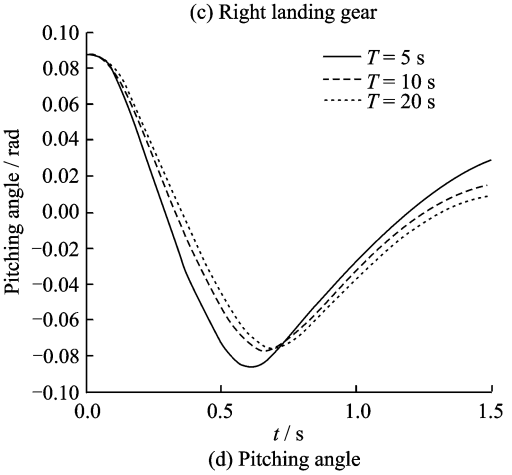

(d) Pitching angle

Fig. 9 Dynamic response of aircraft under different periods of carrier heaving movement

different touchdown patterns. Both smaller pitching angle and landing with a certain rolling angle lead the situation that nose landing gear touches down before main gears; however, the former makes the nose gear landing earlier than both sides of main gears, and the nose gear impact force increases by 168% ($\theta = -6°$); the latter makes nose gear landing earlier than one of the main gears and impact increases by 72.7% ($\gamma = 30°$). The pattern that the nose wheel touches down prior to the main one is dangerous and should be avoided. Meanwhile, the decrease of landing pitching angle enhances the risk of nose landing gear and gains advantage in bolting task.

(2) Effects of the three classic carrier movements on the landing gears impact force vary greatly. The diffidence of pitching initial phase induces that the nose and main gear force increases by 78.7% and 48.28% respectively. From the most influential to the least on the nose and main gear impact loads, the orders are: pitching, rolling, heaving and pitching, heaving and rolling movements separately. Moreover, due to the ship keel center line is not in the aircraft symmetry plane, at the pitching and rolling movement, the change ranges of left and right gear loads are a little different.

(3) Among the effects of the period of carrier movements effect, the rolling affects the impact loads of main landing gears little, but the nose landing gear acutely (when $T = 2$, the nose gear impact load decreases by 60%); the pitching has a great impact on the pitching angle of aircraft while bolting; as the period of rolling varies, the impact loads of nose and right landing gear change in the opposite trend with the left; while pitching and heaving, the impact load of nose landing gear changes in the same trend with the main.

(4) The aircraft landing with a rolling angle and the carrier rolling movement can bring the asymmetric landing of main landing gears, causing the rolling movement of aircraft (the rolling

extent reaches 0.08 and 0.15 respectively), and weakening the hook-cable clench and the arresting performance.

References:

[1] Sherman W L. Generalization and refinement of an automatic landing system capable of curved trajectories[R]. 19770005089. Langley Research Center, 1976.

[2] Riddle D W, Stevens V C. Performance studies on the application of four-engine and two-engine USB propulsive lift to the E-2C aircraft [R]. AIAA 86-2674, 1986:13.

[3] Somieski G. Shimmy analysis of a simple aircraft nose landing gear model using different mathematical methods [J]. Aerospace Science and Technology, 1997, 1(8):545-555.

[4] York B W, Alaverdi O. A physically representative aircraft landing gear model for real-time simulation [R]. AIAA-1996-3506, 1996.

[5] Hu Mengquan, Lin Guohua. Arresting dynamics research of carrier aircraft [J]. Journal of Air Force Engineering University, 2000, 1(5):8-11. (in Chinese)

[6] Wei Xiaohui, Nie Hong. Study on landing impact force of carrier-based aircraft landing gear [J]. China Mechanical Engineering, 2007, 18(5): 520-523. (in Chinese)

[7] Yao Xiongliang, Qu Zuqing, Chen Qifu. Landing loads of airplane gear on the deck of aircraft carrier [J]. Journal of Harbin Engineering University, 1997, 18(2):8-15. (in Chinese)

[8] Zhang Minghui, Yuan Li, Hong Guanxin. Aircraft carrier hydraulic arresting gear arresting force modeling and simulation [J]. Journal of Beijing University of Aeronautics and Astronautics , 2010, 36(1):100-103. (in Chinese)

[9] Zhu Qidan, Wen Zixia, Zhang Zhi. Shipboard arresting kinetic system modeling and simulation [J]. Acta Aeronautica et Astronautica Sinica, 2011, 32(1):1-10. (in Chinese)

[10] Jr Doyle G R. A review of computer simulation for aircraft-surface dynamics [J]. Journal of Aircraft, 1986, 23(4):257-265.

[11] Garza F R. A collection of nonlinear aircraft simulation [R]. NASA TM-212145, 2003.

[12] Nie Hong. Dynamic behavior analysis and design as well as Life prediction method of landing gear [D]. Nanjing: Nanjing University of Aeronautics and Astronautics, 1990. (in Chinese)

[13] Aerospace Industry Ministry of Science and Technology Committee. Handbook of landing gear strength design [M]. Chengdu: Sichuan Science and Technology Press, 1989. (in Chinese)

[14] Smiley R F, Horne W B. Mechanical properties of pneumatic tires with special reference to modern aircraft tires[R]. NASA TR R-64, 1960.

[15] Yang Yidong. Review of the carrier approach criteria [M]. Beijing: National Defense Industry Press, 2006. (in Chinese)

[16] Lu Qian, Li Lianyou, Li Laicheng. Ship principles manual [M]. Beijing: National Defense Industry Press, 1988. (in Chinese)

[17] Yang Yidong. Landing guidance and control of the carrier aircraft [M]. Beijing: National Defense Industry Press, 2007. (in Chinese)

[18] Navy Department of Equipment and Technology. Carrier data handbook [M]. General Design Materials for Carrier Aircraft, 1990.